Supplementary Materials for

Title: Decoding the Function of Expansion Segments in Ribosomes

Authors: Kotaro Fujii[1,2], Teodorus Theo Susanto[1,2], Saumya Saurabh[1], and Maria Barna[1,2,3*]

Affiliations:
[1]Department of Developmental Biology, Stanford University, Stanford, California 94305, USA.
[2]Department of Genetics, Stanford University, Stanford, California 94305, USA.
[3]Lead Contact
[*]Corresponding author: mbarna@stanford.edu

Including
Figures. S1 to S4

Sup_Fig.1

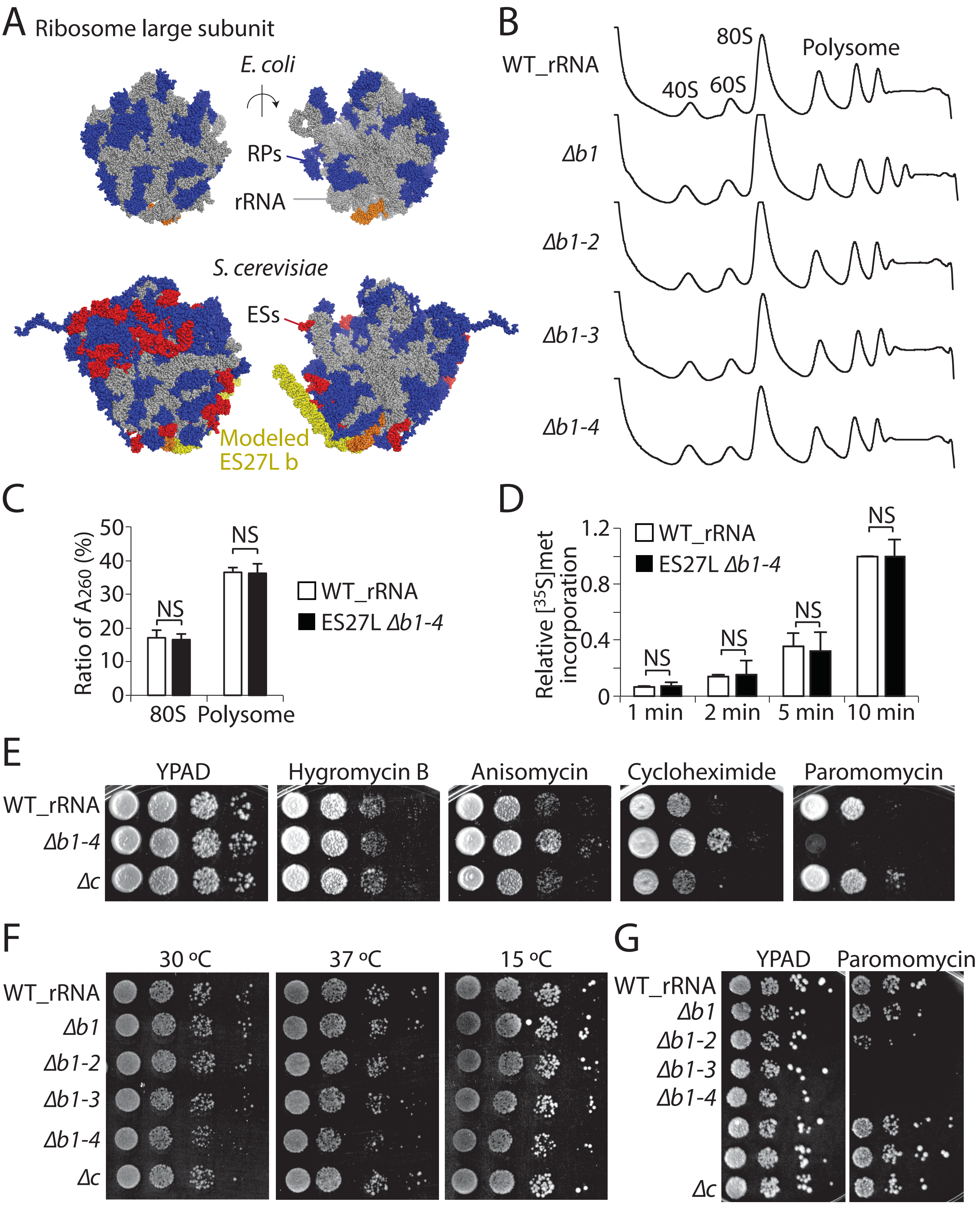
A
Ribosome large subunit
E. coli
RPs
rRNA
S. cerevisiae
ESs
Modeled
ES27L b
B
WT_rRNA
80S
40S
60S
Polysome
Δb1
Δb1-2
Δb1-3
Δb1-4
C
Ratio of A260 (%)
50
40
30
20
10
0
80S
Polysome
NS
NS
☐ WT_rRNA
■ ES27L Δb1-4
D
Relative [35S]met incorporation
1.2
0.8
0.4
0
☐ WT_rRNA
■ ES27L Δb1-4
NS
NS
NS
NS
1 min
2 min
5 min
10 min
E
YPAD
Hygromycin B
Anisomycin
Cycloheximide
Paromomycin
WT_rRNA
Δb1-4
Δc
F
30 °C
37 °C
15 °C
WT_rRNA
Δb1
Δb1-2
Δb1-3
Δb1-4
Δc
G
YPAD
Paromomycin
WT_rRNA
Δb1
Δb1-2
Δb1-3
Δb1-4
Δc

Figure S1. Characterization of ES27L mutant strains in ribosome maturation, global translation, and translation inhibitors or temperature stressors. Related to Figure 1.
(A) The position of the eukaryote specific expansion segments (ESs) (Red) on the ribosome are shown by comparing the large subunit of the *E. coli* (PDB file: 3E1B) and *S. cerevisiae* (PDB file: 4V6I). ES27L "b" and "c" stem-loops are shown (highlighted in yellow), which have been modeled into the Cryo-EM structure (PDB file: 4V6I). The ES27L "a" helix and equivalent stem-loop in *E. coli* are highlighted in orange. Grey: rRNA, Blue: ribosomal protein (RP). (B) Shown are the A_{260} sucrose density profiles of WT_rRNA and ES27L truncated strains revealing that these mutations do not have a big impact on ribosome maturation. (C) The percentage of 80S and polysome fractions over the total A_{260} for WT_rRNA and ES27L Δ*b1-4* strains, revealing that the amount of 80S and polysome do not change between the WT_rRNA and ES27L Δ*b1-4* strain. Data are represented as mean + standard deviation (SD) (*t*-test, $^{**}P < 0.01$; $^{*}P < 0.05$; NS, not significant, $n \geq 3$). (D) The relative amount of [^{35}S]methionine incorporation at log phase in WT_rRNA and ES27L Δ*b1-4* strains show no difference in global protein synthesis rates. Data are represented as mean + SD (*t*-test, $^{**}P < 0.01$; $^{*}P < 0.05$; NS, not significant, $n \geq 3$). (E) The spot assay of WT_rRNA, ES27L Δ*b1-4* and ES27L Δ*c* mutant strains grown on YPAD or plates containing translation inhibitors (25 μg/ml of Hygromycin B, 5 μg/ml of Anisomycin, 0.4 μg/ml of Cycloheximide, or 0.5 mg/ml of Paromomycin) reveals a specific sensitivity of the ES27L Δ*b1-4* strain for Paromomycin. (F) WT_rRNA and ES27L truncated mutant strains were spotted on YPAD plates and subjected to 37 ºC heat shock stress and 15 ºC cold shock stress. (G) Non-trimmed picture of Figure 1B is shown.

Sup_Fig.2

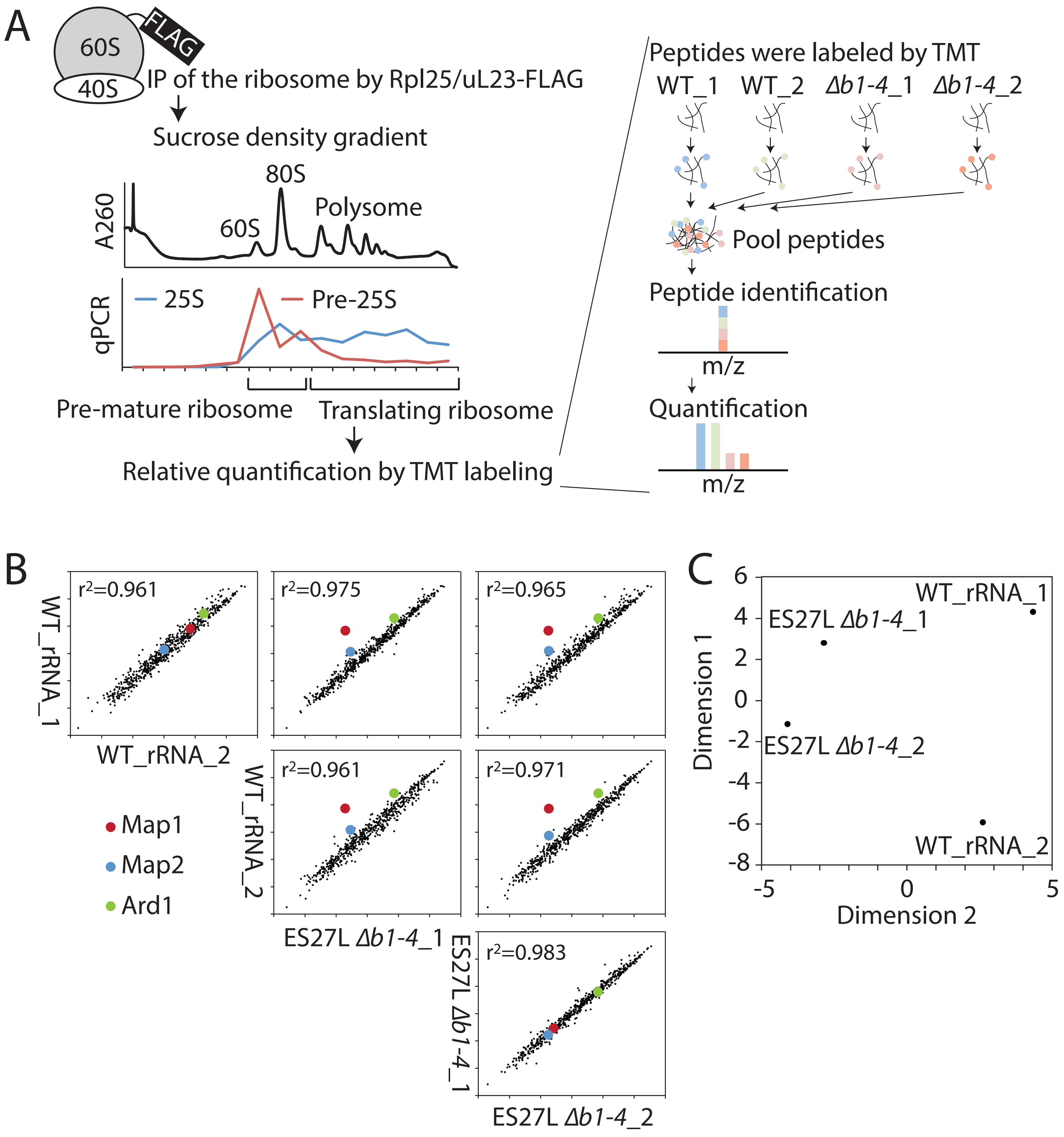
A
60S
40S
FLAG
IP of the ribosome by Rpl25/uL23-FLAG
Sucrose density gradient
A260
80S
60S
Polysome
qPCR
25S
Pre-25S
Pre-mature ribosome
Translating ribosome
Relative quantification by TMT labeling
Peptides were labeled by TMT
WT_1
WT_2
Δb1-4_1
Δb1-4_2
Pool peptides
Peptide identification
m/z
Quantification
m/z
B
r²=0.961
r²=0.975
r²=0.965
WT_rRNA_1
WT_rRNA_2
r²=0.961
r²=0.971
WT_rRNA_2
Map1
Map2
Ard1
ES27L Δb1-4_1
r²=0.983
ES27L Δb1-4_1
ES27L Δb1-4_2
C
6
4
2
0
-2
-4
-6
-8
Dimension 1
WT_rRNA_1
ES27L Δb1-4_1
ES27L Δb1-4_2
WT_rRNA_2
-5
0
5
Dimension 2

Figure S2. Global characterization of the mass spectrometry datasets illustrates the quality of the data. Related to Figure 2.

(A) Schematic workflow of the purification of translating ribosome and subsequent relative quantification mass spectrometry (MS) using Tandem Mass Tag (TMT). Translating ribosomes were purified by immunoprecipitation (IP) using a C-terminal FLAG tagged Rpl25/uL23 followed by sucrose density gradient (SDG) fractionation. To check for contamination of pre-mature ribosomes, RNAs were purified from each fractions and qPCR for pre-mature and total 25S rRNAs were performed. Translating ribosome fractions, free from pre-mature ribosomes, were then combined and proteins were purified. Purified proteins were digested into peptides, labeled with a distinct TMT, combined equally, and subjected to MS analysis. m/z: mass-to-charge ratio. (B) Plots of pairwise correlations of all MS datasets confirm the high consistency in all samples and the change of Map1 (red circle), Map2 (blue circle), and Ard1 (green circle) protein association between WT_rRNA and ES27L Δ*b1-4* strains. (C) Multidimensional Scaling (MDS) analysis reveals clustering of replicates.

Sup_Fig.3

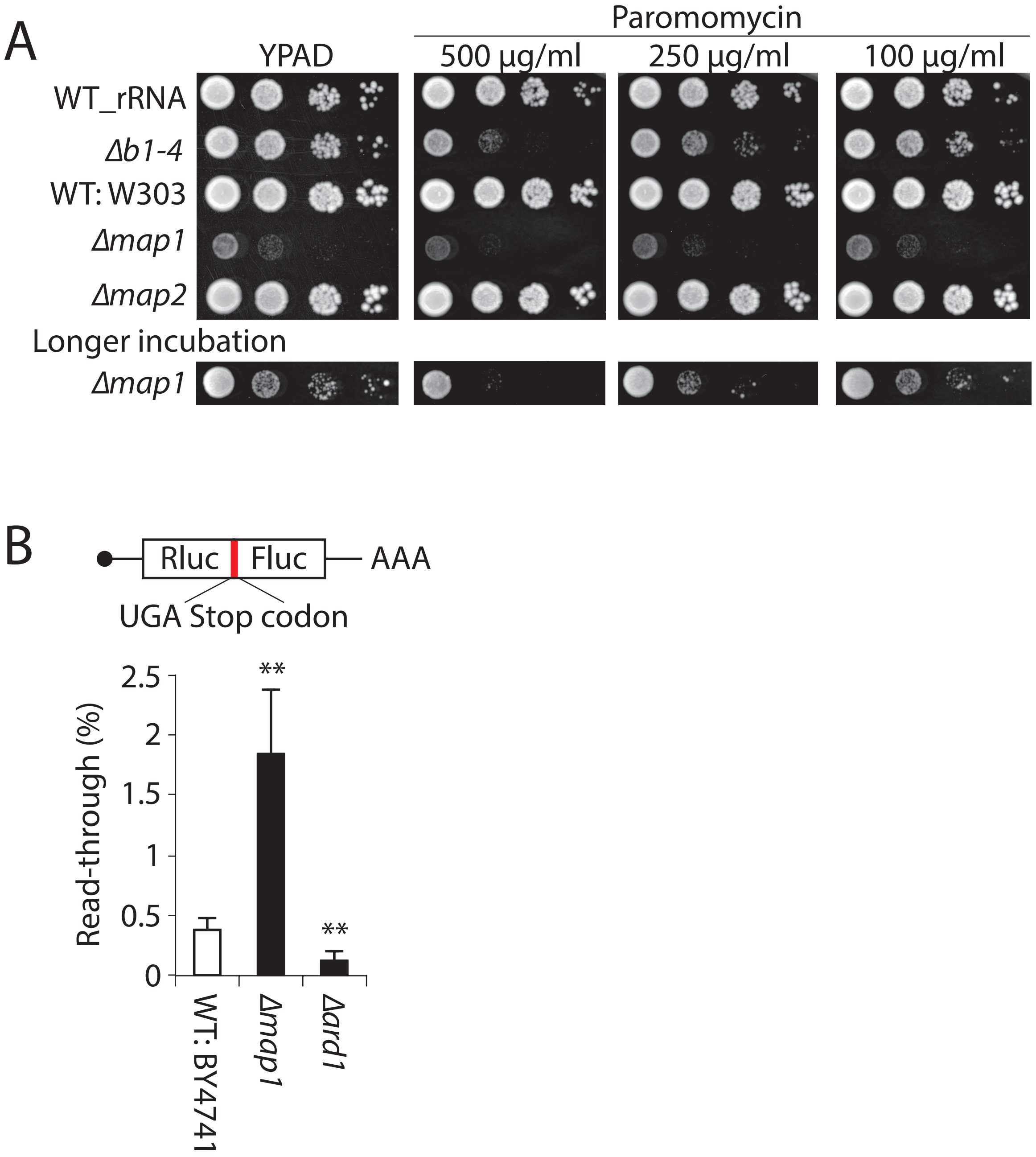
A
Paromomycin
YPAD
500 µg/ml
250 µg/ml
100 µg/ml
WT_rRNA
Δb1-4
WT: W303
Δmap1
Δmap2
Longer incubation
Δmap1
B
Rluc
Fluc
AAA
UGA Stop codon
Read-through (%)
2.5
2
1.5
1
0.5
0
**
**
WT: BY4741
Δmap1
Δard1

Figure S3. The *MAP1* deletion strain phenocopies the ES27L Δ*b1-4* strain for Paromomycin sensitivity, but the NatA subunit component, *ARD1* deletion strain, does not. Related to Figure 3.

(A) Spot assay for indicated strains on plates containing different concentration of Paromomycin shows similar dosage sensitivity between *MAP1* deletion and ES27L Δ*b1-4* strains. Since Δ*map1* strain glow slower, the picture from the longer incubation is also shown.

(B) The translation fidelity of WT (BY4741 background) and *MAP1* or *ARD1* deletion strains were evaluated by the percentage of UGA stop codon read-through. Data are represented as mean + SD (*t*-test, $^{**}P < 0.01$; $^{*}P < 0.05$; NS, not significant, $n \geq 3$).

Sup_Fig.4

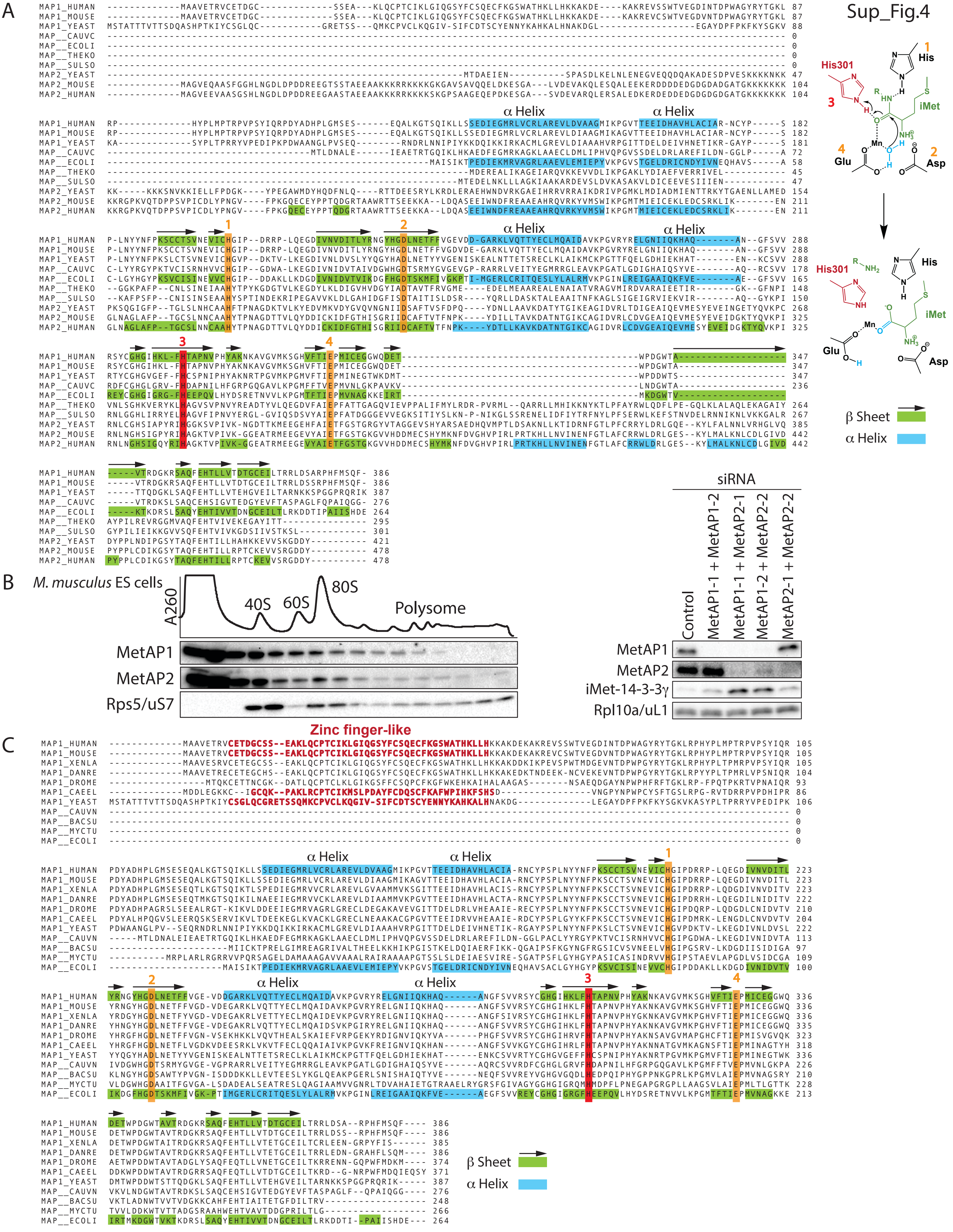
A
MAP1_HUMAN
MAP1_MOUSE
MAP1_YEAST
MAP__CAUVC
MAP__ECOLI
MAP__THEKO
MAP__SULSO
MAP2_YEAST
MAP2_MOUSE
MAP2_HUMAN
α Helix
β Sheet
1
2
3
4
His
His301
iMet
Glu
Asp
Mn
B
M. musculus ES cells
A260
40S
60S
80S
Polysome
MetAP1
MetAP2
Rps5/uS7
siRNA
Control
MetAP1-2
MetAP1-1 + MetAP2-1
MetAP1-1 + MetAP2-2
MetAP1-2 + MetAP2-2
MetAP2-1 + MetAP2-2
iMet-14-3-3γ
Rpl10a/uL1
C
Zinc finger-like
MAP1_XENLA
MAP1_DANRE
MAP1_DROME
MAP1_CAEEL
MAP__CAUVN
MAP__BACSU
MAP__MYCTU

Figure S4. The catalytic amino acids of MetAPs were highly conserved in both Map1 and Map2 proteins. Related to Figure 4.

(A) The catalytic residues of MetAPs are highly conserved in both Map1 and Map2 proteins. Protein alignment of bacterial Map, archaea Map, and eukaryotic Map1 and Map2 from the species listed at the bottom left is shown. Illustration of the enzymatic reaction of MetAP is shown at the right. The catalytic Histidine (His301 in yeast Map1) and the surrounding amino acids are perfectly conserved both in Map1 and Map2 (highlighted in red or orange respectively). Eukaryotic Map1 proteins show higher homology with bacterial Map, while eukaryotic Map2 proteins show higher homology with archaea MAP. α helix (blue) and β sheet (green) structure annotation from the crystal structures of the *H. sapiens* MetAP1 (Addlagatta and Matthews, 2006) and MetAP2 (Liu et al., 1998) as well as *E. coli* Map (Ye et al., 2006) are shown. (B) Sucrose Density Gradient of mouse embryonic stem (ES) cell followed by western blotting for MetAP1, MetAP2, and ribosomal protein (Rps5/uS7) are shown. MetAP1 and MetAP2 antibodies were validated by siRNAs. (C) Eukaryotic Map1 proteins gain an N-terminal extension containing a Zinc finger-like domain. Protein alignment of bacterial Map and eukaryotic Map1 is shown. Zinc finger-like domains annotated in UniProt are highlighted in red. HUMAN: Homo sapiens, MOUSE: Mus musculus, YEAST: Saccharomyces cerevisiae, CAUVN: Caulobacter crescentus, ECOLI: Escherichia coli, THEKO: Thermococcus kodakarensis, SULSO: Sulfolobus solfataricus, XENLA: Xenopus laevis, DANRE: Danio rerio, DROME: Drosophila melanogaster, CAEEL: Caenorhabditis elegans, BACSU: Bacillus subtilis, MYCTU: Mycobacterium tuberculosis.